DRAFT

EBT: AN ALTERNATE CONCEPT TO TOKAMAKS AND MIRRORS*

J. C. Glowienka
Oak Ridge National Laboratory
Oak Ridge, Tennessee 37830

MASTER

*Research sponsored by the Office of Fusion Energy, U. S. Department of Energy, under contract W-7405-eng-26 with the Union Carbide Corporation.

EBT: AN ALTERNATE CONCEPT TO TOKAMAKS AND MIRRORS*

J. C. Glowienka

Oak Ridge National Laboratory

Oak Ridge, Tennessee 37830

ABSTRACT

The ELMO Bumpy Torus (EBT) is a hybrid magnetic trap formed by a series of toroidally connected simple mirrors. It differs from a tokamak, the present main-line approach, in that plasma stability and heating are obtained in a current-free geometry by the application of steady-state, high power, electron cyclotron resonance heating (ECH) producing a steady-state plasma. The primary motivation for EBT confinement research is the potential for a steady-state, highly accessible reactor with high β. In the present EBT-I/S device, electron confinement has been observed to agree with the predictions of theory. The major emphasis of the experimental program is on the further scaling of plasma parameters in the EBT-I/S machine with ECH frequency (10.6, 18, and 28 GHz), resonant magnetic field (0.3, 0.6, and 1 T), and heating power (30, 60, and 200 kW). In addition, substantial efforts are under way or planned in the areas of ion cyclotron heating, neutral beam heating, plasma-wall interactions, impurity control, synchrotron radiation, and divertors. Recently, EBT has been selected as the first alternative concept to be advanced to the proof-of-principle stage; this entails a major device scale-up to allow a reasonable extrapolation to a DT-burning facility. The status and future plans of the EBT program, in particular the proof-of-principle experiment (EBT-P), are discussed.

---

*Research sponsored by the Office of Fusion Energy, U. S. Department of Energy, under contract W-7405-eng-26 with the Union Carbide Corporation.

I. INTRODUCTION

Within the past decade, considerable progress has been made in magnetically confined fusion experiments, but the best magnetic geometry for a reactor has not been identified. The past decade has also seen considerable emphasis placed on the two most successful approaches — tokamaks and mirrors — with a lower emphasis on the less advanced alternatives. In 1978, the Department of Energy initiated a development program to broaden the base of magnetic fusion research by pursuing several of the more promising alternate concepts to a proof-of-principle level. A proof-of-principle experiment is one near enough to the reactor plasma regime to make credible a subsequent progression to a reactor. The first alternate concept so chosen is the ELMO Bumpy Torus (EBT) at Oak Ridge National Laboratory (ORNL). The primary motivation for EBT research is the potential for a steady-state, highly accessible reactor with high β. In this paper we describe EBT through its evolution to the device as it exists today, list its physical characteristics, discuss the relevant plasma characteristics, and outline the important elements of the experimental program, including the proof-of-principle experiment, EBT-P.

II. EBT EVOLUTION

The origins of all magnetic approaches to fusion are to be found in three basic magnetic geometries: the linear solenoid, the simple mirror, and the simple toroid. All three geometries can be maintained in steady state, but they cannot provide a stable equilibrium for the

plasma. The linear solenoid provides no axial confinement. The simple mirror is subject to large axial losses because of loss-cone effects and is susceptible to large radial loss because the region in which the magnetic field curves away from the plasma (field bumps) is unstable to fluid interchange modes. The simple toroid (formed by connecting the ends of the linear solenoid) offers little confinement to even single charged particles, much less a hot dense plasma, because of an inherent radial gradient in the toroidal magnetic field. The field gradient imparts a charge-dependent vertical drift to the particle, sending it to the vacuum wall.

Tokamaks and minimum-B mirrors have emerged from the struggle to find a stable equilibrium. The minimum-B configuration or baseball geometry is made by a magnet whose windings follow the seams of a baseball and can, in principle, be run steady state. The modulus of the magnetic field so produced increases in every direction from the plasma center and stabilizes interchange modes. The tokamak is a low aspect ratio ($R/a \approx 3$) simple toroid through which an intense current is driven. The current generates its own magnetic field, that, when added to the toroidal field, yields a net field that spirals around the torus. Since charged particles are constrained to follow field lines, the net vertical drift can be canceled as the particle moves around the torus. Conventional tokamaks are inherently pulsed devices because the current is driven by transformer action, and, for reactor-scale tokamaks, this might limit each burn pulse to about 1000 to 10,000 seconds. Tokamaks are, however, the most advanced concept in the world, and it appears fairly clear that a tokamak will demonstrate scientific breakeven in this decade.

The ELMO Bumpy Torus (EBT) is a combination of the simple mirror and the simple toroid in a steady-state, current-free configuration. The device is a large aspect ratio ($R/a \geq 10$) toroidally connected set of simple mirrors that does confine single charged particles. The periodic radial gradient in the magnetic field imparts an azimuthal or circular drift to the charged particle and thereby creates the azimuthal mixing for compensation of the verticle drift inherent to a toroid. However, the bumpy torus is still susceptible to MHD activity in the field bumps [1]. For this reason, bumpy tori were rejected as a confinement geometry until a potential solution appeared from mirror research at ORNL.

Throughout the 1960s, a series of simple mirror experiments [2,3] were conducted at ORNL using steady-state microwave power for plasma generation and heating. In the ELMO experiment [3], it was found that very hot ($\geq$500 keV) stable electron ring plasmas were created in the annular region where the applied microwave frequency equalled the second harmonic of the local electron cyclotron frequency ($\omega_\mu = 2\omega_{ce}$) [see Fig. 1]. The stored energy density in the rings ($W_\perp$) was found to be comparable with the local magnetic field energy density (W_b); hence, the ring plasma beta ($\beta \equiv W_\perp/W_b$) was high, as much as 50% in some cases. The diamagnetism of the high-β rings significantly alters the local spatial gradients of the magnetic field, creating a local magnetic minimum or well. By proper choice of the magnetic geometry, these rings can be formed in the regions susceptible to MHD activity, providing a mechanism for stabilization.

The conjecture that the integrated effect of a toroidal series of high-β electron rings, one formed in each field bump, could stabilize the volume equilibrium of a bumpy torus is the genesis of the EBT concept [4]. EBT-I, shown in schematic form in Fig. 2, was constructed (1971-1973) to test this supposition. Experiments began in September 1973 and quickly established that stable, hot (~100 keV), high-β electron rings could be formed in a bumpy torus geometry and that the rings could stabilize a warm, moderately-dense, toroidal core plasma [5].

The primary limit for present EBT particle and energy density is the applied ECH frequency and the available ECH power. After the success of EBT-I using steady-state 18- and 10.6-GHz power, a microwave development program was begun to provide higher frequency, higher power, steady-state sources to examine the scaling of particle and energy densities. The EBT machine is referred to as EBT-I when 18 GHz is used as the primary heating frequency and as EBT-S when 28 GHz is used. The EBT-S experiment uses a 28-GHz gyrotron that, as of May 1980, has operated at the 60-kW level delivering about 30 kW to the core and ring plasmas.

III. MACHINE CHARACTERISTICS

The essential machine features are listed on Table I. The primary vacuum vessel is formed by alternating pieces of mirror sectors and magnets. All vacuum seals are made with Viton O-rings. The vessel is pumped by means of a stainless steel toroidal vacuum manifold that connects to each mirror sector. The manifold is located concentric with, inboard from, and below the horizontal plane of the main vacuum vessel.

Each of the four diffusion pump and refrigerated chevron baffle units connects to the vacuum manifold from below through a ten-inch gate valve.

The ECH power at 10.6 and 18 GHz is fed to each mirror sector by means of a dominant mode waveguide distribution system, and the polarization at the injection port is in the ordinary mode. The 28-GHz ECH power is distributed to each cavity by means of the main pumping manifold which also serves as an overmoded waveguide distribution system. To minimize transmission losses in the manifold, the stainless steel vacuum manifold has been copper plated. Copper overmoded waveguide connects the gyrotron to the manifold.

The use of high-power microwave energy dictated several unique design features. In order to minimize microwave power loss in the primary vacuum vessel, aluminum was chosen rather than stainless steel because the aluminum has a higher conductivity. As a result, Viton O-rings were used rather than hard metal seals. In order to protect the O-rings from the microwave environment, a 4-6 mil step is left on the plasma side of the sealing surface inboard of the O-ring groove. As the bolts are drawn tight, there is no optical path from the microwave environment to the O-ring. All diagnostic openings to the torus are isolated by copper cutoff screens [6] or dielectric absorber (e.g., water). Copper cutoff screens have also been placed directly above each of the four ten-inch gate valves to isolate the pumping system from the microwaves.

EBT, in contrast to tokamaks, is a closed field line device. Field errors as small as 10^{-4} from construction faults and stray fields result in toroidal currents the order of tens of amperes which seriously degrade the single particle confinement of the closed field line geometry [7]. In order to cancel the effect of field errors and to optimize particle confinement, a set of global correction coils has been installed to apply vertical and horizontal correction fields. For the data discussed in the next section, field errors have been compensated by the correction coils.

The high energy ring electrons are eventually lost from the system to the walls and generate a very intense, thick target bremsstrahlung fluence, as high as 1500 R/hr. with present power levels. For personnel protection, EBT is surrounded by 6-inch lead walls and a 4-inch lead roof. When shut down, the machine enclosure can be entered through an optical maze or via a small elevator through the roof. The large-aspect-ratio nature of the machine permits easy access to any part of the machine.

The plasma diagnostics used on EBT are essentially the same diagnostics currently employed on tokamak experiments [8] for measurements of density, temperature, impurities, etc., with one notable addition — a heavy ion beam probe [9-11] to determine the local plasma potential. The steady-state nature of the plasma is ideal for plasma measurements although considerable development effort was required to make some of the tokamak diagnostics work in the hostile EBT environment and at the present low ($\sim 10^{12}$ cm^{-3}) densities. A schematic layout of all the diagnostics and their position on EBT is shown on Fig. 3.

IV. PLASMA CHARACTERISTICS

A. Rings

To stabilize the toroidal core plasma, the rings must form with sufficient stored energy ($W_\perp$) to modify the magnetic field gradients for stabilization of interchange modes. Furthermore, the mirror-confined ring itself must be maintained in a stable equilibrium. Experimental studies [2,3] have found that the threshold value for ring β is about 5-15% regardless of operating point and that the ring is stabilized by cold plasma whose origin is cold gas reflux from the walls. The rings form at the location of the second harmonic resonance ($\omega_\mu \approx 2\omega_{ce}$) with a radial width of a few electron gyroradii and an axial length comparable to the plasma radius. Theoretical calculations using fluid and kinetic formalisms [12-17] predict the experimentally observed threshold, equilibrium, and stability conditions.

The operational mode is determined by the microwave power and the background neutral pressure. There are three distinct modes observed: C for cold, T for toroidal, and M for mirror [5]. The C-mode is characterized by a relatively high electron density (approaching cutoff) but a low core electron temperature ($\sim$ 10 eV) and no appreciable hot electron ring (little stored energy). The T-mode is characterized by the existence of high-β, hot electron rings, an electrostatic potential well within the core and improved confinement manifested in higher core temperatures ($\geq$100 eV) at moderate densities. The M-mode is characterized by a very tenuous and unstable plasma, and steady-state operation is not possible. The dependence of line integrated density $n_{e\ell}$, stored energy $W_\perp$, and electrostatic potential well depth ΔV_p on background neutral pressure is

shown on Fig. 4a which displays the three operating modes for constant ECH power and magnetic field. The rim of the potential well ($\gtrsim$ 100 V) is located in the region of the annulus and defines the radius of the stabilized core plasma as shown on Fig. 4b. The potential rim and annulus location (crosshatched) follow the location of the second harmonic resonance as the magnetic field is changed.

An analysis of the bremsstrahlung distributions emitted by the hot electrons yields the ring temperatures and densities. As shown on Fig. 5a, significant improvement in ring parameters is realized by increasing the ECH frequency. The range of points at each frequency corresponds to a range in experimental conditions (e.g., power, neutral density, and ring position). For a given microwave frequency (and magnetic field), the ring temperature is almost constant with changing pressure (or power) as seen on Fig. 5b. On the other hand, the density increases as the neutral density decreases (or as the microwave power increases). The variation in stored energy as seen in Figs. 4a and 5a with pressure (or power) is partially due to the variation in ring density. Additional variations may be due to changes in the ring volume; however, these changes have not been measured. Figure 5a demonstrates that ring temperature increases more with microwave frequency (resonant magnetic field B_r) than does the density, as expected from ring scaling models [2,18-20].

The microwave power required to sustain the rings in EBT-I/S is modest ($\sim$5-10 kW) and reasonably well estimated by recently developed theoretical models [19,21], which include as power loss mechanisms drag

cooling, Coulomb scattering, and synchrotron radiation. The drag losses dominate the lower range of the ring energy ($T_{ring} \leq 1$ MeV), but decrease as $T_{ring}^{-1/2}$. At high ring energies ($T_{ring} \geq 2$ MeV), accelerated ring cooling occurs because of the synchrotron radiation. Studies [2] indicate that the parameters important for the total power loss are: ring beta; ratio of cold-to-hot plasma density required for ring stability [15]; magnetic field at the annulus (B_r); fraction of microwave cutoff; and ring volume. The models indicate that the ring-sustaining power will be a significant but not an overriding factor in EBT reactor economics [19].

A comparison of ring parameters from the heirarchy of relevant experiments, ELMO, NBT (the Nagoya Bumpy Torus, see Ref. 22), and EBT-I/S suggest that most dimensionless ring parameters as required by models (e.g., those mentioned above) are nearly constant or vary in the direction of increased stability. The near constancy is of great utility for extrapolation to future devices like the proof-of-principle experiment and a reactor [23].

B. T-mode plasma

The local magnetic wells produced by the high-beta, hot electron annuli allow the equilibrium volume of the bumpy torus to be filled stably with a warm, dense toroidal core plasma. A summary of typical EBT-I/S T-mode plasma parameters is shown on Table II. Spatial profiles of electron temperature and density from Thomson scattering are flat; preliminary ion temperature profile data from charge exchange indicate a flat profile or a slight peaking at plasma center. Experimental evidence

of the quiescent nature of the T-mode plasma is seen on a plot (Fig. 6a) of the normalized, line-integrated fluctuation level of H_α light (656.3 nm) as a function of background neutral pressure at constant ECH power. Also plotted for reference is $n_e\ell$ from Fig. 4a. A spatially resolved plot (Fig. 6b) of the H_α fluctuation level in the T-mode indicates that the residual fluctuations occur in the unstabilized regions outside of the ring (shown in crosshatch).

Confinement of plasma in the nonaxisymmetric EBT geometry differs fundamentally from that in (near) axisymmetric geometries such as tokamaks. An ambipolar electric field arises to balance the diffusion rates for ions and electrons because of the pronounced nonaxisymmetric magnetic field shape, and it is, therefore, of fundamental importance to measure the plasma potential as a function of position. The radial potential plot shown on Fig. 4b indicates a potential well nearly symmetric about a point 4 cm inside the toroidal axis. The inward shift is consistent with the shift theoretically predicted for the plasma due to the radial gradient of the toroidal magnetic field. The rim is approximately co-located with the hot electron annulus. The ambipolar electric field inside the rim is also nearly symmetric about this point, points radially inward, and is of sufficient magnitude to strongly influence azimuthal particle drifts. The symmetry shown in Fig. 4b is critically dependent on global nulling of the field errors [7] and on having T-mode conditions. For example, in the C-mode, the absolute potentials are smaller, and the potential well and symmetry are lost.

Another unique feature of the T-mode plasma is that it is relatively free of impurities. Line radiation in the vacuum ultraviolet was measured to determine the density of impurities and their spatial distributions [24]. The primary impurities found in EBT are aluminum and carbon.

Examining the particle balance and the spatial profiles of carbon, values of the product of electron density n_e and impurity lifetime τ_j were determined for two radial positions at the surface of the plasma and listed in Table III. In this region, the electron density has an average value of about 3×10^{11} cm^{-3}, and the confinement time is considerably less than 10^{-3} sec. In effect, the surface plasma acts like a divertor to ionize incoming neutral impurities and directs them to the walls before they diffuse into the toroidal plasma. The divertor effect is enhanced by the presence of the large positive potential barrier observed at the position of the hot electron annulus (Fig. 4b).

Some impurities will reach the toroidal core, but their densities are very low as illustrated in Table IV. The fractional amount of all carbon in the core is less than 6×10^{-5}, which illustrates the effectiveness of the surface plasma in reducing the toroidal impurities. The aluminum concentration is somewhat larger (same order of magnitude) because the aluminum can directly enter the core plasma from sputtering at the mirror throats. Furthermore, despite the steady-state nature and the potential well, impurities do not accumulate in the core plasma. There are turn-on transients lasting several minutes; however, the signal eventually saturates at the levels shown in Table IV.

Recent experimental emphasis has been to obtain complete data sets using all diagnostics simultaneously for use in self-consistent neoclassical transport calculations [25,26]. One measure of EBT confinement properties is the comparison of the particle diffusion coefficient D_{ne} calculated using experimentally derived values with those obtained from a bounce-average kinetic equation [25]. Table V displays data sets [27] from NBT, EBT-I, and EBT-S that were used in the calculations. The agreement of theory and experiment shown on the lower part of Table V is within a factor of 2 when allowance is made for experimental accuracy. Likewise, values of theoretically and experimentally derived electron power balance can be compared, and good agreement is again obtained indicating neoclassical electron behavior. Also shown on Table V are the calculated values for energy confinement time and the density-confinement time product.

The ions present a more complicated picture. The measured ion charge-exchange spectrum has three energy groups [28] including a cold component (<30 eV), a component representing the bulk ion temperature (~70 eV), and a high energy tail (~400 eV). With a potential well depth typically greater than 200 eV, it is mainly ions in the tail population, which represents about 1% of the total ion distribution, which have enough energy to diffuse over the potential barrier. The bulk ions are trapped in the potential well. However, a problem arises in ion power balance calculations because it is easily demonstrated that more power is lost via charge exchange than is input via Coulomb collisions with electrons. This implies a source of additional ion heating power such

as wave heating. Futher theoretical and experimental studies are under way to better understand these mechanisms.

V. EBT PROGRAM

Past programmatic effort has emphasized the development of a complete array of spatially resolved plasma diagnostics. With this array operational, the experimental program has now turned to power scaling studies. Experiments will begin shortly wherein the ECH power deposited in the plasma is in excess of 100 kW, the goal being 200 kW from one 28-GHz gyrotron. Engineering work has already begun to install a second unit, doubling the available ECH power to 400 kW.

The ions are only indirectly heated by ECH through the electrons. An intense collaborative effort is under way with industry to directly heat the ions with ion cyclotron heating (ICH). Experiments will begin shortly using up to 20-kW steady state in the range from 2-20 MHz and plans are to have up to 200 kW available sometime in the middle of FY 81. Intense neutral beam heating is also a proven way to deliver energy directly to the ions, but steady-state, high-power injectors do not exist. Furthermore, simple calculations indicate problems with particle inventory because the steady-state fluence would quickly outstrip any known pumping system and charge-exchange losses will be high. A low intensity diagnostic neutral beam is being installed for spatially resolved ion temperature measurements and to examine the compatibility of neutral injectors in the microwave environment. A divertor effort, again in collaboration with industry, is being conducted to study the

problem of pumping, particle inventory and fueling. Impurity control, although not presently necessary, may be required in larger, hotter devices like EBT-P.

The major focus of the EBT program is, of course, the proof-of-principle device EBT-P. As mentioned above, experimentally confirmed neoclassical behavior provides the scaling formalism necessary to design the device, the essence of which is

$$n\tau_e \sim A^2 \, T_e^{3/2} \, (1 + \frac{e\varphi}{T_e})^2$$

where,

$n\tau_e$ = density-confinement time product for the electrons

A = aspect ratio $\approx$ major radius R/minor radius a

T_e = electron temperature

φ = potential

In addition, the density is limited by microwave cutoff (electron plasma frequency $\leq$ electron cyclotron frequency) and therefore scales as

$$n_{max} \propto f_\mu^2 \propto B_r^2 \quad .$$

The resonance occurs in the region between the coils, and for a mirror ratio of about 2, the maximum magnetic field at the coil is approximately twice B_r. With a performance goal broadly taken to be a steady-state, PLT-like plasma with $n\tau \sim 10^{12}$ cm^{-3} sec, EBT-P will be a major scale-up in physical size and operating parameters from the EBT-I/S machine.

A reference design [29] has emerged from an intense design effort [30,31] that has involved ORNL and four industrial consortia [32] in competition to be chosen as ORNL's industrial participant for final design, procurement, construction, and operation of EBT-P. A summary of the reference design parameters and performance compared with those of EBT-I/S is shown on Table VI. It is well recognized that such performance will not be obtained immediately, but rather through a series of staged upgrades, hence the notation EBT-PI. For example, it is proposed to start at 60 GHz, but to have the magnet capability to accommodate as high as 90-GHz ECH power. This increase in frequency should lead to a factor of two improvement in $n\tau$ from density alone.

An attempt to display the significance of pulse length t_p in a comparison of EBT and tokamak performance is shown on Fig. 7. Present tokamaks operate for not more than 1 sec; TFTR has the capability for about 10-sec operation. The ETF, as a tokamak, is projected to have a pulse length of 100 sec. A tokamak reactor may be expected to operate for about 10,000 sec. The present EBT-I/S operates in excess of 10,000 sec (about 4 hours), limited mainly by operator fatigue.

That EBT-P has, in its improved state, the potential for achieving parameters such as $n\tau \geq 10^{12}$ cm^{-3} sec, $T_i > 1$ keV at $n > 10^{13}$ cm^{-3} with $\beta \geq 5\%$ in steady state is remarkably significant even when compared with achievements and projections of other devices.

REFERENCES

[1] KADOMTSEV, B.B., Reviews of Plasma Physics, Vol. 2 (1966) 153.

[2] UCKAN, N.A., Chairman and Editor, EBT Ring Physics (Proc. of the Workshop, Oak Ridge, TN, 1979) ORNL CONF-791228, Oak Ridge (1980).

[3] DANDL, R.A., et al., in Plasma Physics and Controlled Nuclear Fusion Research (Proc. 3rd Int. Conf. Novosibirsk, 1968) II, IAEA, Vienna (1969) 435; Plasma Physics and Controlled Nuclear Fusion Research (Proc. 4th Int. Conf. Madison, 1971) II, IAEA, Vienna (1972) 607; and DANDL, R.A., "Review of Ring Experiments," in Ref. [2], pp. 31-57.

[4] DANDL, R.A., et al., in Plasma Physics and Controlled Nuclear Fusion Research (Proc. 6th Int. Conf. Berchtesgaden, 1976) II, IAEA, Vienna (1977) 145.

[5] DANDL, R.A., et al., in Plasma Physics and Controlled Nuclear Fusion Research (Proc. 7th Int. Conf. Innsbruck (1978) II, IAEA, Vienna (1979) 365; Oak Ridge National Laboratory Report, ORNL-TM-4941 (1975) and ORNL/TM-6457 (1978).

[6] The cutoff screens have holes sized smaller than required for wave propagation cutoff but have approximately 70% optical transmission for pumping.

[7] QUON, B.H., et al., Oak Ridge National Laboratory Report, ORNL/TM-6740 (1979).

[8] EQUIPE TFR, Ed. by DE MICHELIS, C., Nucl. Fusion 8 (1978) 647.

[9] JOBES, F.C., HICKOK, R.L., Nucl. Fusion 10 (1970) 195.

[10] COLESTOCK, P.L., et al., Phys. Rev. Lett. 40 (1978) 1717.

[11] BIENIOSEK, F.M., et al., Rev. Sci. Instrum. 51 (1980) 206.

[12] ARD, W.B., DANDL, R.A., STETSON, R.F., Phys. Fluids 9 (1966) 1498.

[13] GUEST, G.E., HEDRICK, C.L., NELSON, D.B., Oak Ridge National Laboratory Report, ORNL-TM-4077 (1972).

[14] BERK, H.L., Phys. Fluids 19 (1976) 1255.

[15] DOMINGUEZ, R.R., BERK, H.L., Phys. Fluids 21 (1978) 827; DOMIGUEZ, R.R., "Flute Interchange Stability in a Hot Electron Plasma," in Ref. [2], pp. 383-407.

[16] NELSON, D.B., HEDRICK, C.L., Nucl. Fusion 19 (1979) 283.

[17] OWEN, L.W., HEDRICK, C. L., DELEANU, L.E., Oak Ridge National Laboratory Report, ORNL/TM-7388 (to be published).

[18] UCKAN, N.A., Oak Ridge National Laboratory Report, ORNL/TM-7302 (1980) (submitted to Nucl. Fusion).

[19] BOROWSKI, S.K., UCKAN, N.A., JAEGER, E.F., KAMMASH, T., Nucl. Fusion 20 (1980) 177.

[20] BATCHELOR, D.B., "Microwave Heating of the Annulus in EBT," in Ref [2], pp. 261-287.

[21] See Ref. [2], pp. 319-379 and pp. 503-523.

[22] In 1978, EBT was joined by a companion electron cyclotron heated bumpy torus — the Nagoya Bumpy Torus (NBT), Institute of Plasma Physics, Nagoya University, Nagoya, Japan.

[23] UCKAN, N.A., et al., in Plasma Physics and Controlled Nuclear Fusion Research (Proc. 7th Int. Conf. Innsbruck, 1978) III, IAEA, Vienna (1979) 343.

[24] LAZAR, N.H., et al., Nucl. Fusion 19 (1979) 571.

[25] SPONG, D.A., et al., Nucl. Fusion 19 (1979) 665.

[26] JAEGER, E.F., et al., Nucl. Fusion 19 (1979) 443; Nucl. Fusion 19 (1979) 1627.

[27] FUJIWARA, M., et al., Paper IAEA-CN-38/BB-4, 8th Int. Conf. on Plasma Physics and Controlled Nuclear Fusion Research, Brussels, 1980.

[28] DANDL, R.A., EBT Transport (Proc. of Workshop, A. Kadish, Ed.), U. S. Department of Energy, DOE/ET-0112 (1979) 1.

[29] BOCK, A.L., "EBT-P Proposed Reference Design Report," Oak Ridge National Laboratory Report, ORNL/TM-7179 (1980).

[30] DANDL, R.A., et al., Oak Ridge National Laboratory Report, ORNL/TM-5955 (1978).

[31] BOCK, A.L., et al., Oak Ridge National Laboratory Report, ORNL/TM-7066 (October 1978).

[32] The four consortia are headed by EBASCO, Grumman, McDonnell-Douglas, and Westinghouse.

TABLE I. EBT-I/S MACHINE PARAMETERS

Basic Machine

Major radius	150 cm
Magnet throat radius	11.1 cm
Cavity sector radius	25.4 cm
Aspect ratio	9

Vacuum System

Toroidal tank volume	1350 ℓ
Vacuum manifold volume	560 ℓ
Pumping	4 - 10-inch diffusion pumps, Santovac 5 oil, refrigerated Chevron baffles
Net pumping speed	5000 ℓ/sec
Base pressure	$\sim 5 \times 10^{-7}$ torr

Gas Feed

Any gas, primarily hydrogen, pressure controlled by a feedback controlled piezo valve

Cavity Sectors

Number	24
Material	Aluminum, 6061T6, normal machine finish

Magnets

Number	24
Mirror ratio on axis	2:1
Conductor	Normal copper (water cooled)
Construction	4 Pancakes wound 3-in-hand
Max. current	9000 A steady state
Field strength on axis (throat/midplane)	
EBT-I	1 T/0.5 T @ 6 MW cw
EBT-S	1.4 T/0.7 T @ 12 MW cw
Magnet case	Aluminum 2219T352, normal machine finish

Electron Cyclotron Heating System

Frequency (GHz)	Source	Total Power (kW cw)
10.6	3 Klystrons	30
18	4 Klystrons	60
28	1 Gyrotron	60 (presently)

TABLE II. TYPICAL EBT-I/S PLASMA PARAMETERS IN T-MODE

	EBT-I	EBT-S
n_e (cm^{-3})	$\leq 10^{12}$	$1\text{-}2 \times 10^{12}$
T_e (eV)	250-400	400-600
T_i (eV)	30-80	60-90
$\Delta\phi$ (volts)	80-300	140-550

TABLE III. PRODUCT OF ELECTRON DENSITY WITH CARBON ION DENSITY ($n_e n_j$) AND ION LIFETIME ($n_e \tau_j$) IN THE SURFACE PLASMA REGION OF EBT

Species	Radius	$n_e n_j$ (cm^{-6})	$n_e \tau_j$ (cm^{-3} sec)
C II	10	0.61×10^{20}	
	15	0.46×10^{20}	
C III	10	0.51×10^{20}	3.2×10^{7}
	15	0.36×10^{20}	3.2×10^{7}
C IV	10	0.49×10^{19}	4.4×10^{7}
	15	0.34×10^{19}	4.4×10^{7}

TABLE IV. IMPURITY ION DENSITIES IN THE REGION OF THE TOROIDALLY CONFINED PLASMA

($n_e = 2 \times 10^{12}$ cm^{-3})

Ion Charge State	Density (cm^{-3}) at r = 0
C II	5.9×10^{7}
C III	3.9×10^{7}
C IV	1.0×10^{7}
C V	$< 1.4 \times 10^{7}$
Al II	4.7×10^{7}
Al III	1.3×10^{8}

TABLE V. EXPERIMENTAL DATA SET

Experimental Values		NBT	EBT-I	EBT-S
Mirror ratio/aspect ratio		1.9:1/8:1	2:1/9:1	2:1/9:1
B_r	(T)	0.3	0.65	1.0
Bulk heating power	(W)	3×10^4 (8.5 GHz)	5×10^4 (18 GHz)	4.4×10^4 (28 GHz)
Profile heating power	(W)	1×10^4 (10.5 GHz)	2×10^4 (10.6 GHz)	5×10^3 (18 GHz)
Power to core plasma	(W)	$\sim 5 \times 10^3$	$2.8\text{-}11.4 \times 10^3$	$(6.9\text{-}10) \times 10^3$
Average core plasma radius	(m)	0.06-0.09	0.077	0.068
Major radius R	(m)	1.6	1.5	1.5
Central density n	(m^{-3})	$3\text{-}5 \times 10^{17}$	10^{18}	$(1.2\text{-}2) \times 10^{18}$
Central electron temp. $T_e(0)$	(eV)	50-140	250	~ 500
Central ion temp. $T_i(0)$	(eV)	-	80-90	~ 100
Ion tail temp T_t	(eV)	-	~ 400	~ 400
Potential well depth V_p	(V)	50-70	~ 190	~ 250
Neutral density n_o	(m^{-3})	$(0.5\text{-}1) \times 10^{16}$	$(0.25\text{-}1) \times 10^{16}$	$(0.25\text{-}1) \times 10^{16}$
Calculated Values				
D_{ne} experiment	($m^2 s^{-1}$)	0.19-1.2	0.16-0.65	0.17-0.7
D_{ne} theory	($m^2 s^{-1}$)	0.12-0.82	0.34	0.24-0.4
τ_E	(s)	$(2\text{-}4) \times 10^{-4}$	$(1\text{-}3.4) \times 10^{-3}$	$(2.7\text{-}4.1) \times 10^{-3}$
$n\tau_E$	($m^3 s$)	$(0.6\text{-}2) \times 10^{14}$	$(1\text{-}3.4) \times 10^{15}$	$(3.2\text{-}8.0) \times 10^{15}$

TABLE VI. EBT-P REFERENCE DESIGN PARAMETERS

	EBT-I	EBT-S	EBT-P	EBT-PI
B_{res} (T)	0.64	1.0	2.1	~ 3.2
R (m)	1.5	1.5	4.5	4.5
A	9.3	9.3	16	16
$\bar{a}$ (m)	0.11	0.11	0.18	0.18
N_{coils}	24	24	36	36
n (cm^{-3})	1.5×10^{12}	4×10^{12}	1.7×10^{13}	$\sim 5 \times 10^{13}$
T_e (keV	0.2	0.5	2	~ 5
T_i (keV)	0.06	0.1	~ 0.4	~ 2
$n\tau$ (cm^{-3}/sec)	1×10^{10}	2×10^{10}	5×10^{11}	$\sim 5 \times 10^{12}$

FIGURE CAPTIONS

FIG. 1. A cross-sectional view of ELMO showing magnetic flux lines and the approximate position of the mirror-confined hot electrons.

FIG. 2. Drawing of the ELMO Bumpy Torus.

FIG. 3. Schematic diagram of diagnostics and their location on EBT-I/S.

FIG. 4a. Line integral density $n_e\ell$ and potential well depth ΔV_p as a function of ambient neutral pressure in EBT-I. Also shown is the stored ring energy, $W_\perp$.

FIG. 4b. Horizontal radial scan of space potential for various magnetic field strengths (1 ampere = 1 gauss midplane on axis). The location of the second harmonic resonance is shown as a hatched region.

FIG. 5a. Experimental variation of ring temperature and density with ECH frequency.

FIG. 5b. Experimental variation of ring density and temperature with ambient neutral pressure at constant power.

FIG. 6a. Normalized line integrated fluctuations of H_α light (656.3 nm) as a function of ambient neutral pressure. Also plotted for reference is $n_e\ell$ from FIG. 4a.

FIG. 6b. Location of H_α light fluctuations with respect to hot electron ring (shown by hatched region).

FIG. 7. $n\tau$ versus T_i versus t_p.

ORNL-DWG 76-8119

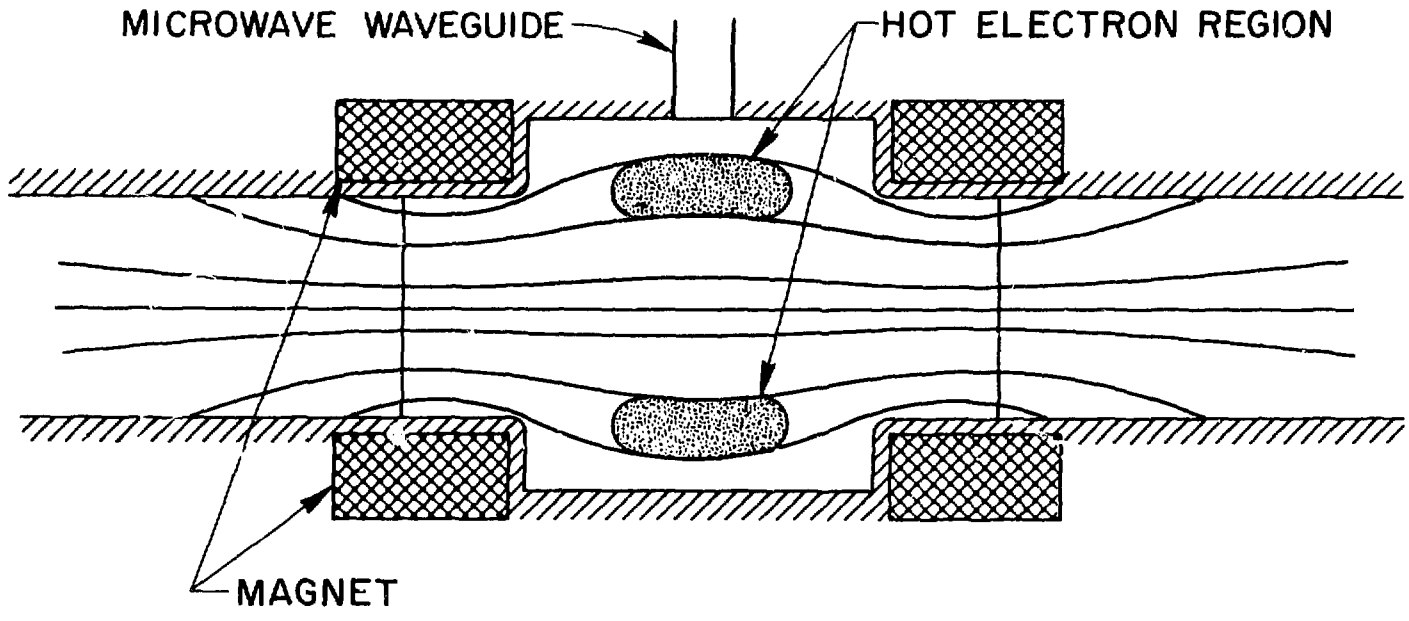

ORNL DWG 73-5045R5

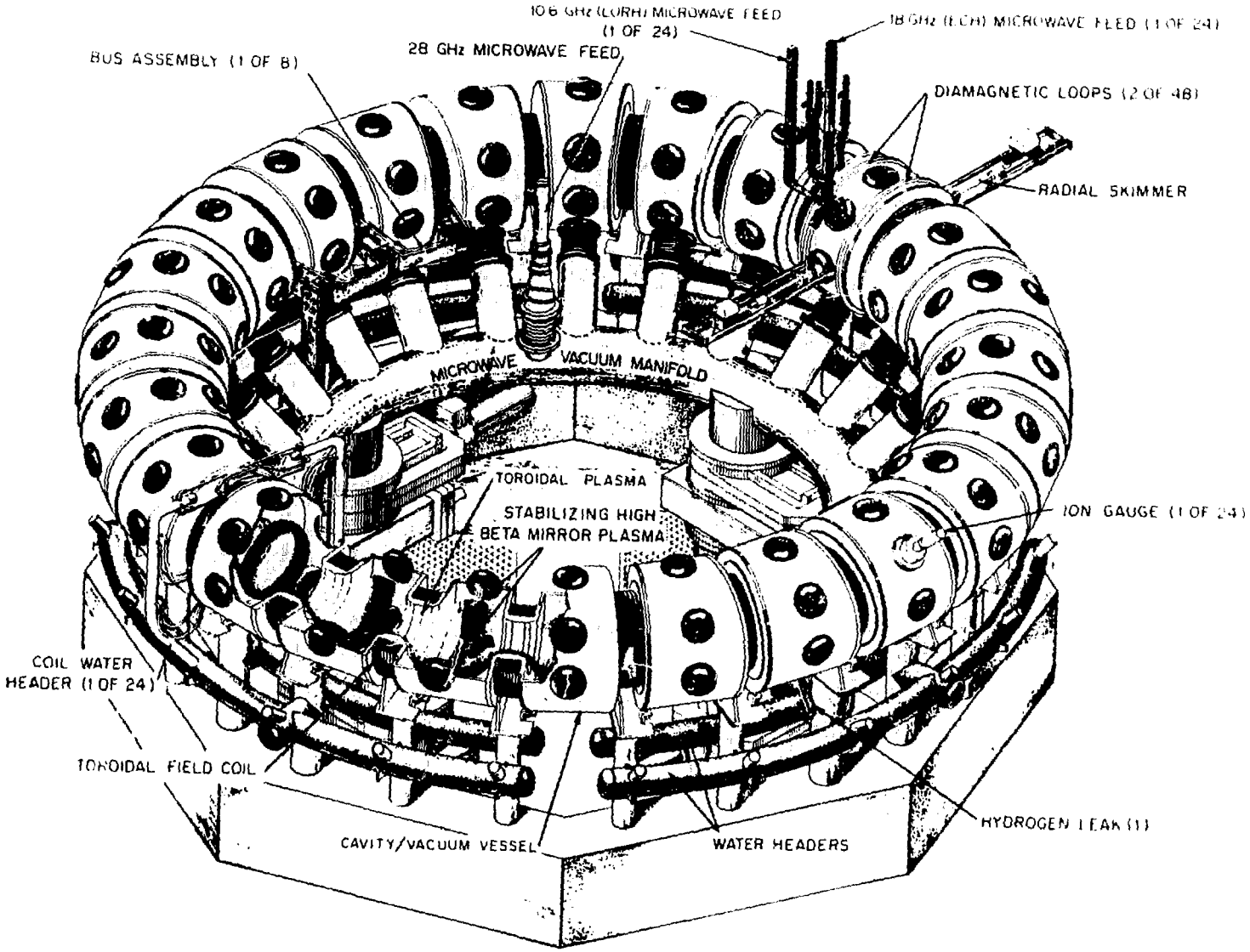

DIAGNOSTICS ON EBT-I/S 1980

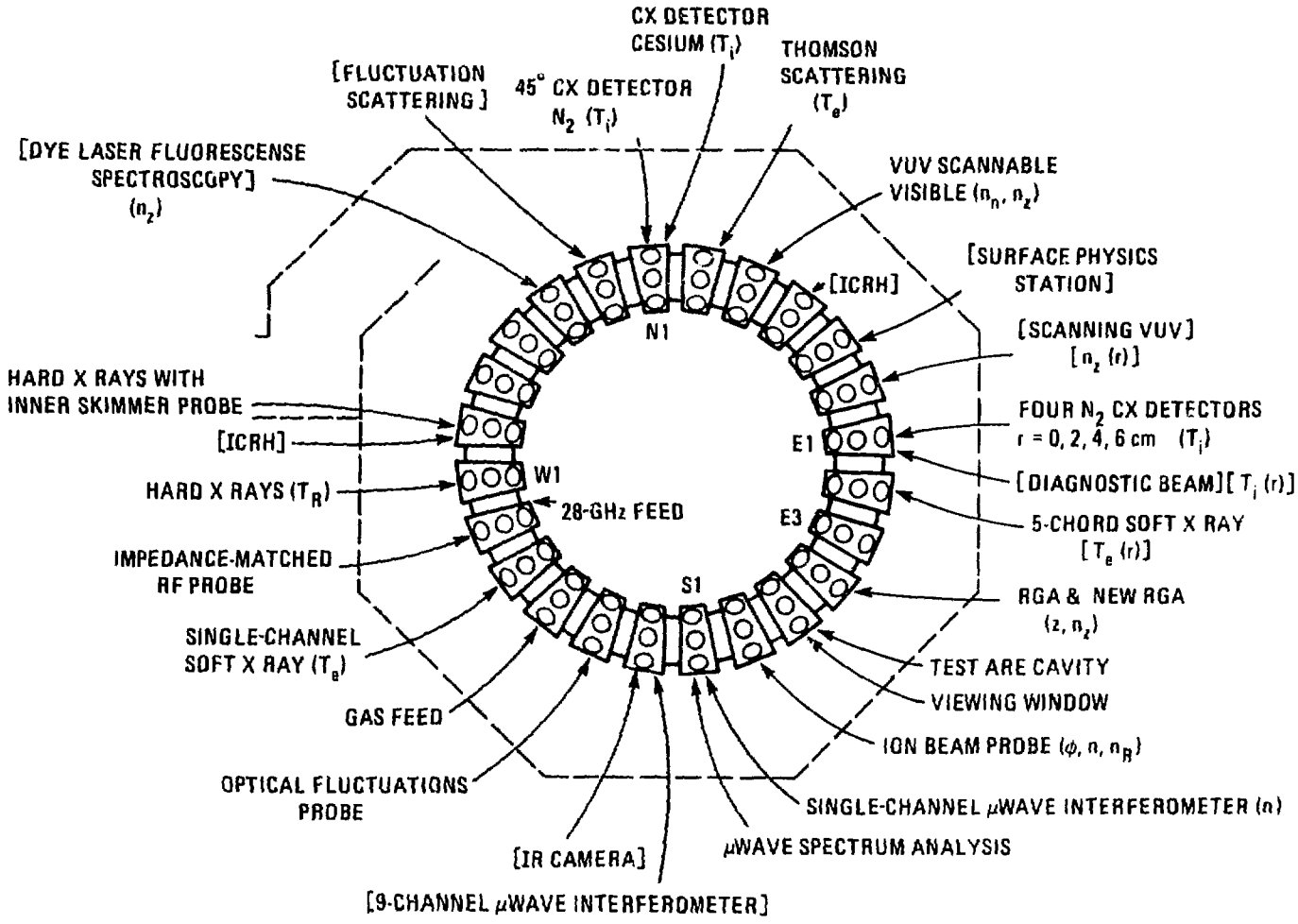

BRACKETS MEAN NOT INSTALLED AT PRESENT

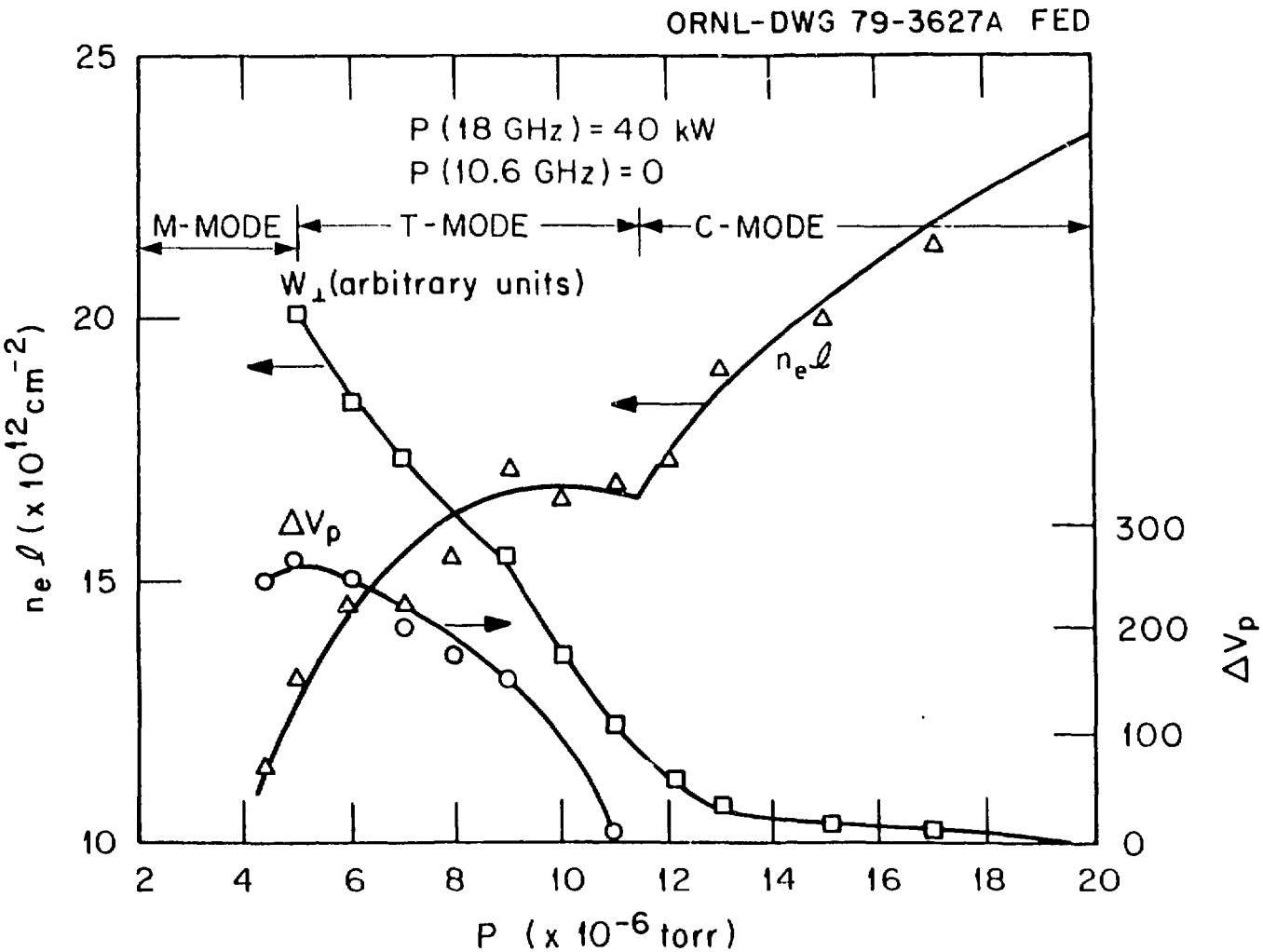
ORNL-DWG 79-3627A FED
P (18 GHz) = 40 kW
P (10.6 GHz) = 0
M-MODE
T-MODE
C-MODE
W⊥(arbitrary units)
$n_e\ell$
ΔV_p
$n_e\ell$ (x 10^{12} cm^{-2})
ΔV_p
P (x 10^{-6} torr)
25
20
15
10
300
200
100
0
2
4
6
8
10
12
14
16
18
20

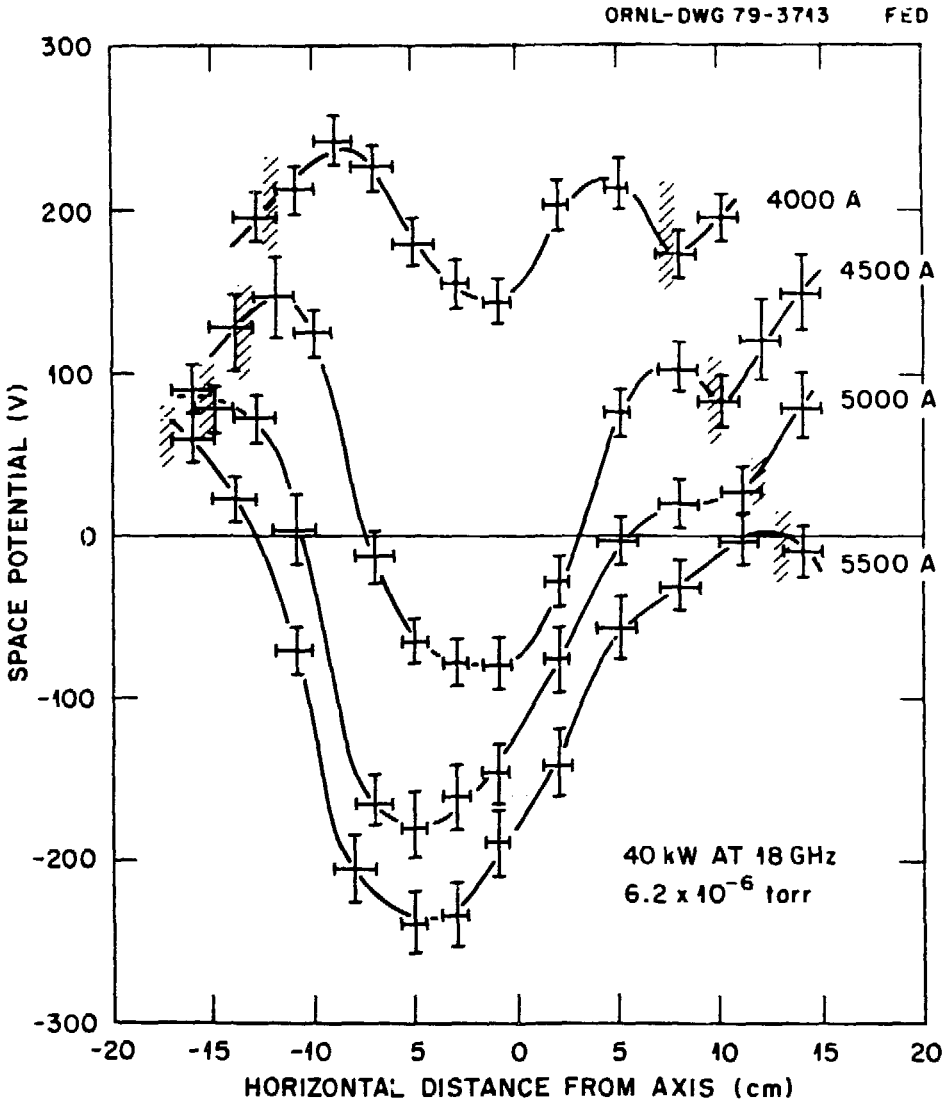
ORNL-DWG 79-3713 FED
300
200
100
0
-100
-200
-300
SPACE POTENTIAL (V)
4000 A
4500 A
5000 A
5500 A
40 kW AT 18 GHz
6.2 x 10⁻⁶ torr
-20
-15
-10
5
0
5
10
15
20
HORIZONTAL DISTANCE FROM AXIS (cm)

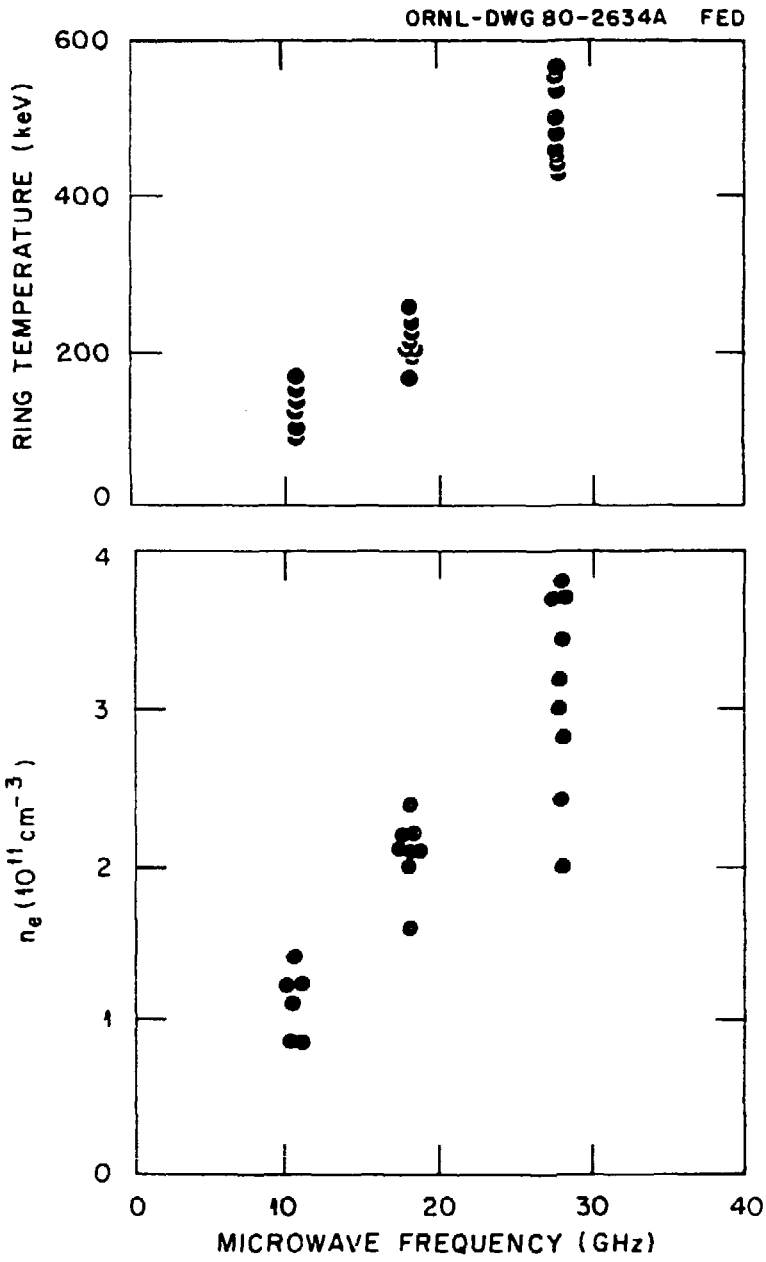
ORNL-DWG 80-2634A FED
RING TEMPERATURE (keV)
600
400
200
0
$n_e (10^{11} cm^{-3})$
4
3
2
1
0
0
10
20
30
40
MICROWAVE FREQUENCY (GHz)

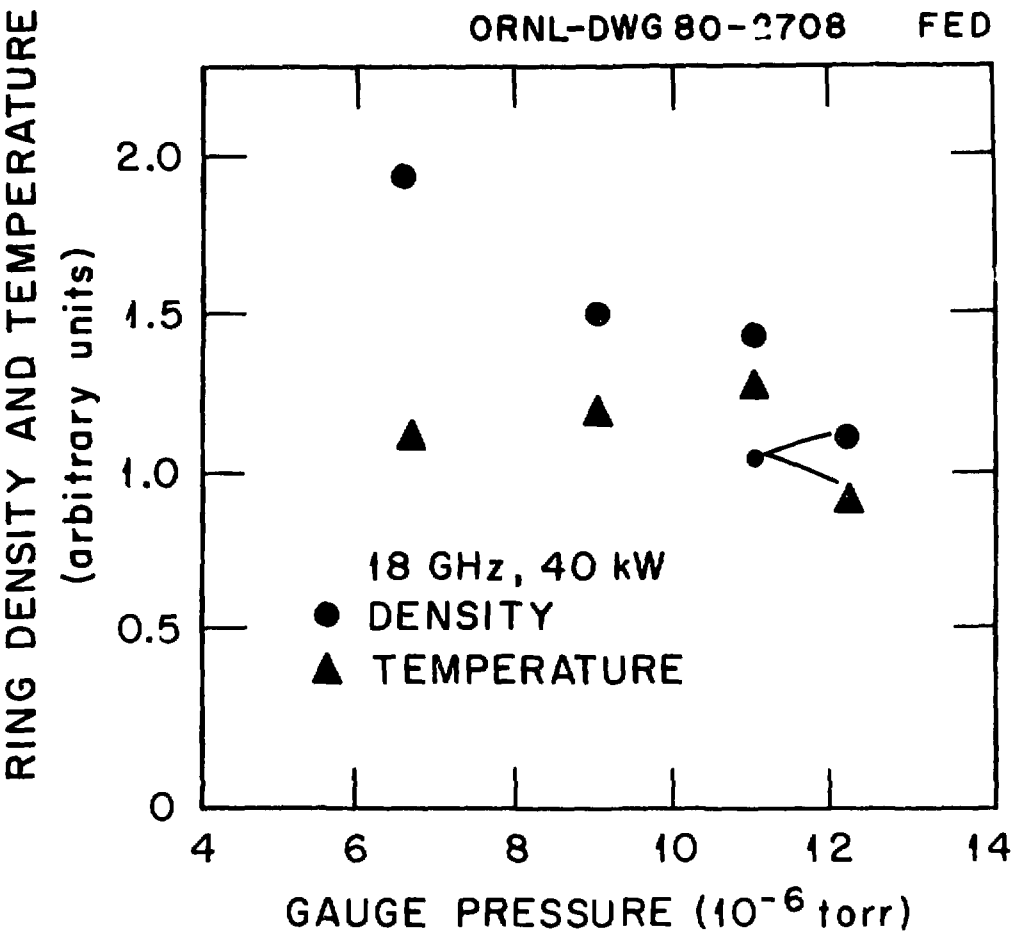
ORNL-DWG 80-2708 FED
RING DENSITY AND TEMPERATURE
(arbitrary units)
2.0
1.5
1.0
0.5
0
4
6
8
10
12
14
GAUGE PRESSURE (10^{-6} torr)
18 GHz, 40 kW
DENSITY
TEMPERATURE

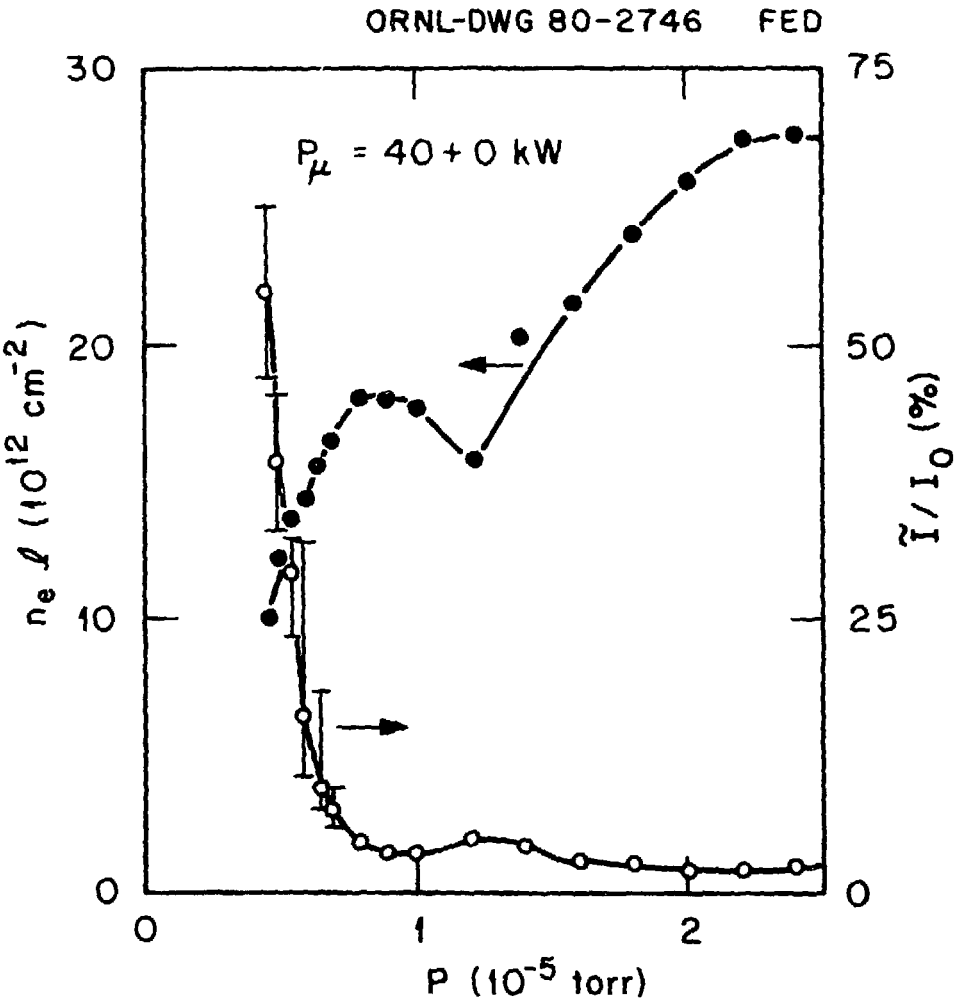
ORNL-DWG 80-2746 FED
P_μ = 40+0 kW
$n_e \ell$ (10^{12} cm^{-2})
$\tilde{I}/I_0$ (%)
P (10^{-5} torr)
30
20
10
0
75
50
25
0
0
1
2

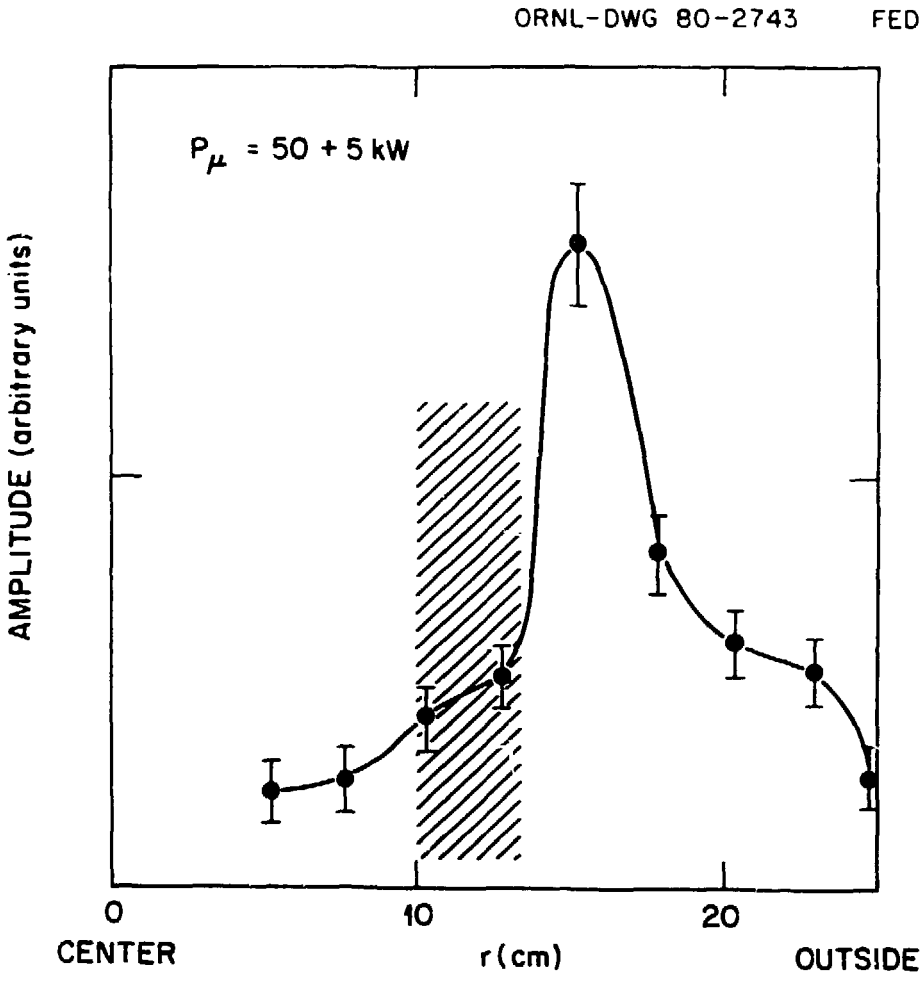
ORNL-DWG 80-2743 FED
P_μ = 50 + 5 kW
AMPLITUDE (arbitrary units)
0
10
20
CENTER
r (cm)
OUTSIDE

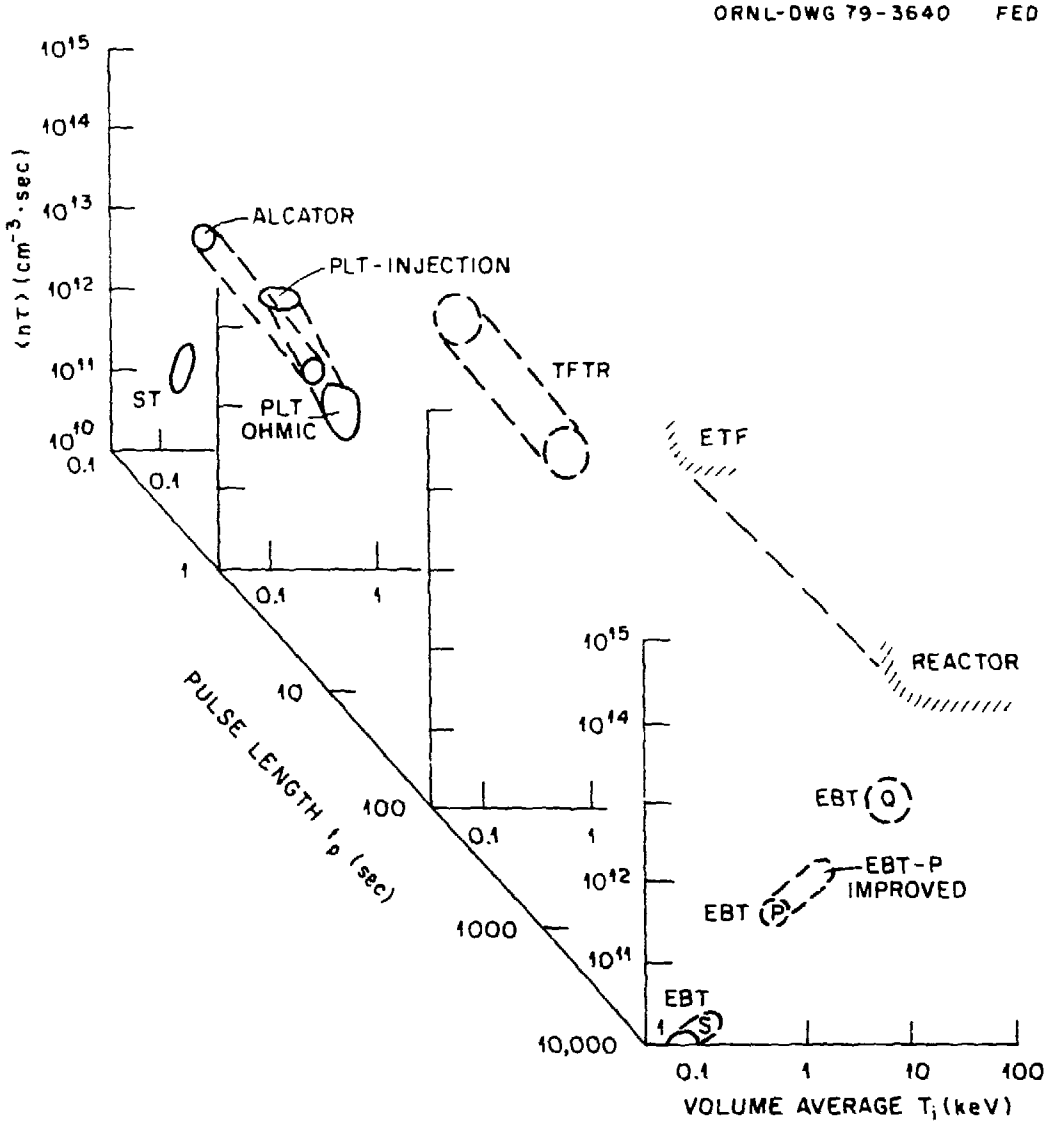
ORNL-DWG 79-3640 FED
10^{15}
10^{14}
10^{13}
10^{12}
10^{11}
10^{10}
$\langle nT \rangle$ (cm^{-3} · sec)
ALCATOR
PLT-INJECTION
TFTR
ST
PLT
OHMIC
ETF
REACTOR
EBT (Q)
EBT-P
IMPROVED
EBT (P)
EBT
(S)
0.1
1
10
100
1000
10,000
PULSE LENGTH t_p (sec)
VOLUME AVERAGE T_i (keV)